

A new way to explain the 511 keV signal from the center of the Galaxy and experimental search for small hydrogen

J. Va'vra

SLAC, Stanford University, CA94309, U.S.A.
e-mail: jjv@slac.stanford.edu

Abstract – The first detected gamma-ray line originating from outside the solar system is the 511 keV emission from the center of our Galaxy. The widely accepted explanation attributes this signal to electron-positron annihilation. However, despite over 30 years of extensive theoretical and observational research, the primary sources of these positrons remain unidentified.

In this paper, we propose an alternative explanation: the observed signal arises from atomic transitions involving a “small hydrogen atom,” where an electron is captured into a tightly bound orbit around a proton. We review the current status of experimental searches for small hydrogen, both in astrophysical data and laboratory experiments, and propose new methods for its direct detection in the lab. Additionally, we explore whether small hydrogen could be a candidate for dark matter.

Key words: 511 keV peak at the galactic center, small hydrogen atom, DDL atom, dark matter

INTRODUCTION

Rutherford suggested already in 1920 that electron-proton could be bound in tight state [1]. At that point neither the Shroedinger equation (1926) nor Dirac equation (1928) was known to him. He asked his team, including Chadwick, to search for this atom. After Chadwick's discovery of the neutron in 1932 there was a lot of discussions whether it is an elementary particle or a hydrogen-like atom formed from electron and proton [2]. For example, Heisenberg was among those who argued that Chadwick's particle is a small hydrogen atom until 1933. At the end the Pauli's argument won, that the neutron spin 1/2 follows Fermi-Dirac statistics and this decided that the neutron is indeed an elementary particle. **This is a well-established fact and it is not discussed in this paper.**

However, it is a separate question to see if the relativistic Schrödinger (Klein-Gordon or K-G) or Dirac equations would actually allow a solution corresponding to a small hydrogen, which would be a completely separate entity to the neutron discovered by Chadwick. It must have been obvious to both Schrödinger and Dirac, and certainly to Heisenberg, that there is a peculiar solution to their equations. This particular solution, which corresponds to the small hydrogen, Schiff [3] rejected because the wave function is infinite at $r = 0$. The infinity comes from the Coulomb potential shape, which has the infinity at $r = 0$; it was a consequence of the assumption that the nucleus is point-like. In addition nobody has observed it. At that point the idea of small hydrogen died. However, its idea was revived again ~70-years later by Maly and Va'vra [4,5,6], where

authors argued that the proton has a finite size, being formed from quarks and gluons, and that the electron experiences a different non-Coulomb potential at very small radius – see Fig.1. Authors of Refs.[4,5,6] argued that the rejected solution should be accepted because the electron's orbit inside or close to proton is not subject to the Coulomb potential force; instead, it is subject to force of a different potential.

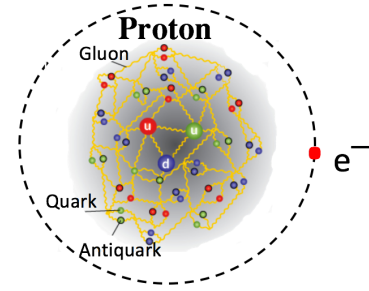


Figure 1 A schematic view of small hydrogen atom. Electron is on deep level of small hydrogen at a radius $r \sim 1.42$ Fermi and proton radius is ~ 0.877 Fermi. Electron does not feel point-like Coulomb potential at this radius.

In fact, such non-Coulomb potentials are used in relativistic Hartree-Fock calculations for very heavy atoms where inner shell electrons are close to nucleus [7,8]. Maly and Va'vra simply applied a similar idea to the problem of small hydrogen, i.e., they used the Coulomb potential in the relativistic Schrödinger and Dirac equations to solve the problem outside the nucleus first, then they used the above mentioned **non-Coulomb potentials** in a separate solution for small radius, and then matched the two solutions at a certain radius; one should note that probably more sophisticated potentials will have to be used in the future as the proton quark structure is complex. Using this method they retained solutions for small hydrogen which were previously rejected. It is interesting to note that the difference between two types of hydrogens, a normal-size and a small-size, is only a sign in one equation. One should point out that Refs.[4,5] did not consider the relativistic virial theorem.

S. Brodsky argued that one should not use the "1920-30 quantum mechanics" to solve the problem of small hydrogen because the electron becomes relativistic; instead, one should use, for example, the Salpeter-Bethe (S-B) theory [9]. He also pointed out that there were earlier attempts to find a tight electron-proton bound state using the QED S-B theory [10], which includes spin-spin, field retardation term and Coulomb potential, assuming the point-like proton; reference [10] hints

that if the retardation term is dropped, there is no bound state, or resonance as they call it (they did not estimate its lifetime).

Quantum mechanics does allow all sort of strange atomic states in nature composed of various particles, some observed, but mostly unstable. Table 1 shows several examples of such states.

Table 1: Strange atomic states

(a) QED predicted large states [11]:

Name	Status
Muonium (μ^+e^-)	Observed, unstable
Di-muonium ($\mu^+\mu^-$)	Not yet observed
Di-taonium ($\tau^+\tau^-$)	Not yet observed
Muonic hydrogen ($p\mu^-$)	Observed, unstable
Muonic helium ($He-\mu^-$)	Observed, unstable
Large positronium (e^+e^-)	Observed, unstable
Di-positronium molecule ($(e^+e^-)^2$)	Observed, unstable
Protonium ($p\bar{p}$)	Not yet observed

(b) Small states suggested in this paper:

Small hydrogen (pe^-)	Not observed
Small positronium (e^+e^-)	Not observed
Small muonium ($\mu^+\mu^-$)	Not observed

There are two reasons why the idea of small hydrogen was not investigated theoretically further: (a) nobody has found it experimentally, and (b) the theory at small distance from proton is too complicated.

This paper will not try to resolve this issue theoretically properly, it provides only theoretical hints. Instead we turn to experimental observations seeking any hint of evidence for the existence of such atoms, hoping that if they are found experimentally, the real theory can be developed.

In this paper, we make an **ansatz** that small hydrogen exists. One can immediately ask a question why we do not observe spontaneous transitions between normal atomic levels and deep electron orbits.¹ In other words, why we are here? I propose a simple explanation: an electron, to latch on a deep electron level, must have a very high energy, which cannot be obtained from the Coulomb potential energy alone. To form this atom, I believe, this energy must be “supplied” to electron **externally**, similarly to electron capture on proton. This can happen only in high energy physics experiments, or in very violent events occurring in Universe, but not spontaneously or in simple bench-top experiments.

There are two major possibilities to consider: (a) small hydrogen is stable with lifetime comparable to the age of Universe, (b) small hydrogen is not stable. In this case, atomic transitions to deep levels are still possible, but the small hydrogen atom would decay immediately with some time constant.

The paper is organized as follow. Chapter 1 will present several non-QED methods to calculate the small hydrogen problem: (a) Solutions using calculations based on relativistic Schrödinger and Dirac equations. (b) Solutions based on iterative virial theorem calculation based on a simple relativistic Bohr-like model. The overall aim here is to point out that these states might exist to motivate theorists to solve it properly (Bohr model, despite its simplicity, yielded many useful results, which

then helped to trigger quantum mechanics revolution). The two approaches, (a) and (b) are yielding somewhat different results, but they both hint that small hydrogen may exist.

Chapter 3 discusses various possible methods how to discover the small hydrogen: (a) searching for ep-bonded state in high energy physics experiment, (b) searching for small hydrogen in large sparks in hydrogen, (c) suggesting that the 511 keV signal at the center of our galaxy is due to the small hydrogen formation, (d) searching Sun’s optical spectra for its spectral signature, (e) detection of relativistic small hydrogen produced by Blazars, (f) suggestion that the small hydrogen is formed during supernova explosions, and (g) searching for its hyperfine signal. **The suggestion that the small hydrogen is produced during the supernova explosions is crucial to our argument.**

Chapter 5 discusses a question if **small hydrogen could be the Dark Matter particle satisfying SIDM models**. The standard model of dark matter, called Cold Dark Matter (CDM), allows the particles to interact mainly through gravity. An example of CDM particle is WIMP. A new model, called Self-Interacting Dark Matter (SIDM) has become a popular alternative to explain some phenomena. This model assumes that dark matter particles interact via gravity but also among themselves, and with surprisingly high cross-section.

Chapter 6 points out that young galaxies may behave differently than the old galaxies in terms of the long orbital velocity tail, which hints to us that the dark matter, in this case the small hydrogen, is being produced by the galaxy itself.

1. Motivation to search for small hydrogen atom

1.1. The 1920-30 quantum mechanics argument.

Authors of Refs.[4,5,6] made a point that accepting the previously rejected solution, and made these conclusions: (a) radius of small hydrogen is only a few Fermi in size, (b) Table 2 shows that energy levels¹ are between 507-511 keV [4].

Table 2 - Energy levels of small two small atoms [4]

(a) Relativistic Schrödinger (Klein-Gordon) levels (pe^-)

Spectroscopic labeling	n	ℓ	m	E_{DDL} [keV]
1s	1	0	0	-507.27
3p	3	1	1	-509.76
5d	5	2	2	-510.26

* n, ℓ , m are quantum numbers

(b) Dirac levels for small hydrogen (pe^-)

Spectroscopic labeling	N	M	K	L1	E_{DDL} [keV]
2s	2	1	1	0	-509.13
4p	4	2	2	1	-510.06
6d	6	3	3	2	-510.38

(c) Dirac levels for small positronium (e^+e^-)

Spectroscopic labeling	N	M	K	L1	E_{DDL} [keV]
2s	2	1	1	0	-254.566
4p	4	2	2	1	-255.032
6d	6	3	3	2	-255.166

* n, l, m, and N, M, K, L1 are quantum numbers.

To illustrate an argument of Maly and Va’vra [4] in favor of small hydrogen, we show an example of their solution for the relativistic Schrödinger (Klein-Gordon) equation for hydrogen-like atoms (following Schiff [3]):

¹ Maly and Va’vra called these “deep” levels Deep Dirac Levels (DDL levels).

$$(-\hbar^2 \nabla^2 + m^2 c^2)u(\vec{r}) = [E - e\phi(r)]^2 u(\vec{r}) \quad (1)$$

This equation can be solved exactly for the Coulomb potential $e\phi(r) = -Ze^2/r$ by using: $u(r, \theta, \phi) = R(r) Y_{lm}(\theta, \phi)$, which yields the radial equation:

$$\frac{1}{\rho^2} \frac{d}{d\rho} \left(\rho^2 \frac{dR}{d\rho} \right) + \left[\frac{\lambda}{\rho} - \frac{1}{4} - \frac{l(l+1) - g^2}{\rho^2} \right] R = 0 \quad (2)$$

where $\rho = ar$, $g = Ze^2/\hbar c$, $\alpha^2 = 4(m^2 c^4 - E^2)/(\hbar^2 c^2)$, and $\lambda = 2Eg/(\hbar c \alpha)$. The solution can be obtained by the following substitution:

$$R(\rho) = F(\rho) e^{-\frac{\rho}{2}},$$

$$\text{where } F(\rho) = \rho^s (a_0 + a_1 \rho + a_2 \rho^2 + \dots) = \rho^s L(\rho)$$

This leads to this differential equation:

$$\rho^2 \frac{d^2 L(\rho)}{d\rho^2} + \rho[2(s+1) - \rho] \frac{dL(\rho)}{d\rho} + [\rho(\lambda - s - 1) + s(s+1) - l(l+1) + g^2] L(\rho) = 0 \quad (3)$$

Putting explicitly $L(\rho)$ function into equation (3), one obtains:

$$[s(s+1) - l(l+1) + g^2] a_0 \rho^0 + f_1(s, l, g) \rho^1 + f_2(s, l, g) \rho^2 + \dots = 0$$

Equating each term in front of each ρ^n with zero, one obtains from the very first term ρ^0 :

$$s(s+1) + g^2 - l(l+1) = 0 \quad (4)$$

which is a quadratic equation with the following solution:

$$s = -\frac{1}{2} \pm \left[\left(l + \frac{1}{2} \right)^2 - g^2 \right]^{\frac{1}{2}} = s(\pm) \quad (5)$$

There are two solutions with two infinities:²

- 1) For $s = s(+)>0$: $F(\rho) \rightarrow \infty$ as $\rho \rightarrow \infty$
To keep $F(\rho)$ finite one sets $\lambda = \text{integer} + s + 1$
- 2) For $s = s(-)<0$: $F(\rho) \rightarrow \infty$ as $\rho \rightarrow 0$
This solution was neglected in the past.

The present quantum mechanics allows $s(+)$ solution. One can ask why $s(-)$ solutions were neglected? A simple answer is by quoting Schiff [3]: “The boundary condition that wave function $F(\rho)$ be finite at $\rho = 0$ requires that we choose positive solution $s(+)$ ”; in other words, the wave function cannot be normalized at $\rho = 0$; however, Maly and Va’vra argued that Schiff was assuming a point-like proton, which is clearly not the correct assumption.

References [4,5] proposed that near $\rho=0$ one should use a combination of the Coulomb potential and either Nix or Smith-Johnson potential. Figure 3c shows an example of the Nix potential, which has a finite value at $\rho=0$. The idea was to solve the problem in two separate regions, use the relativistic Schrödinger equation outside of nucleus using Coulomb potential and some other potential inside, and match two solutions at some boundary (In chapter 1.3 we will show that one needs a stronger potential than Coulomb potential at small radius to satisfy virial theorem).

References [4,5] calculated energy levels, for small the $s(-)$ hydrogen states, using the relativistic Schrödinger equation as

developed by Schiff [3] (equation 53.16, page 470):³

$$E_{\text{Relativistic Schrödinger}} = \frac{mc^2}{\sqrt{(1+g^2/(n'+s+1)^2)}} \quad (6)$$

where $s = s(-)$ and $n' = 0, 1, 2, \dots$

Similarly, $s(-)$ hydrogen states for the Dirac equation follows Flügge [12] (eq. 202.17, page 198):

$$E_{\text{Dirac}} = \frac{mc^2}{\sqrt{[1+g^2/(s+n')^2]}} \quad (7)$$

where $s = s(-)$ and $n' = 0, 1, 2, \dots$

Energy levels from these two formulas are shown graphically on Figure 2. One can see that for orbital excitations above $k \sim 10$ the transition energy becomes to be very close to ~ 511 keV for large k . Since it is likely that transitions to DDL levels are accompanied with large orbital excitations, one could assume that typical single photon will have energy close to 511 keV.

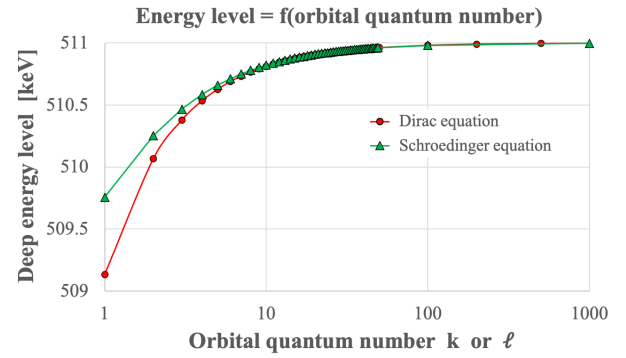


Figure 2 DDL energy levels approach a value of -511 keV, as k or ℓ increases, using equations (6) and (7).

It is interesting to note that energy levels are determined by requirement that infinite series must be terminated at $\rho \rightarrow \infty$, where on the Coulomb potential is dominating. The small radius region does not contribute to energy level. However, as we will see later, one must introduce a stronger potential than Nix potential at small radius to hold the small hydrogen stable.

Once the electron energy is known using equations (6-7), one can estimate corresponding radius of small hydrogen using Bohr's approximation: $r_{Bohr} = 0.5 KZe^2/E$, where energy E is calculated using equations (6) and (7). This method of calculating radius is for illustration only; a proper way is to determine wave functions and plot a probability distribution of electron position as a function of radius. Figures 3a&b show radial and energy distributions for ground state of small hydrogen using Coulomb and $V_{(Spin.B)}$ potential (see chapter 1.4) one can see that the most probable energy is about ~ 140 MeV and that this distribution is very broad. Fig.3c shows a combination of Coulomb, Nix, $V_{(Spin.B)}$, V_{eff} and hard ball potentials (see chapters 1.4 & 1.5). One can clearly see that $V_{(Spin.B)}$ and V_{eff} potentials are much stronger than Coulomb or Nix potentials in the region between 1-20 Fermi.

² Quantum mechanics allows only integer quantum numbers. They are needed to terminate a solution in a form of infinite series. No fractional quantum numbers are allowed in standard quantum mechanics.

³ Formula (6) with $s = s(+)$ was first derived by Sommerfeld in 1916.

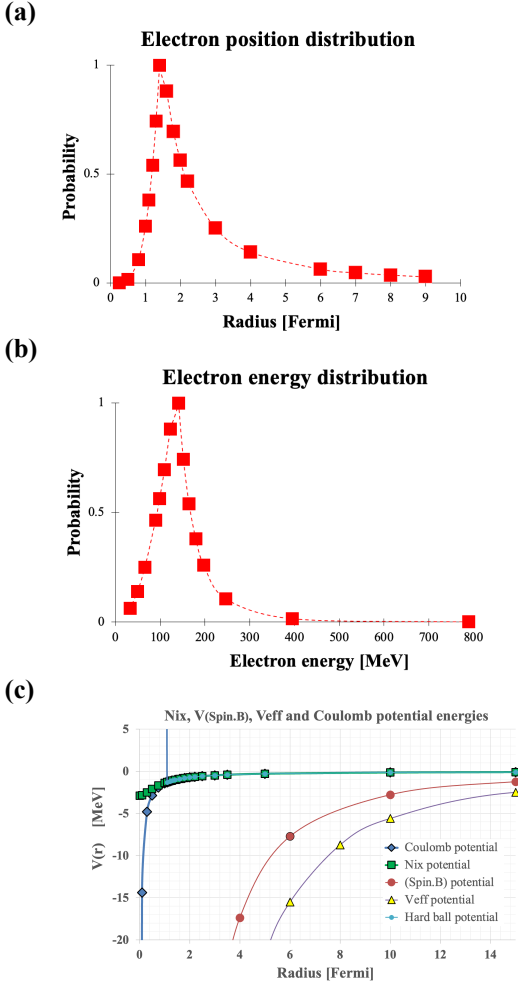


Figure 3 (a) Radial and (b) energy distribution of electrons in small hydrogen atom in ground state for a combination of Coulomb and Nix potentials as determined by Maly and Va'vra [5]. (c) Shapes of Coulomb, Nix, $V(\text{Spin.B})$, V_{eff} and hard ball potentials (see discussion in later chapters).

Although the Maly and Va'vra [4,5] predicted small hydrogen energy levels, **they did not prove that (a) the small hydrogen is stable with their chosen potentials, and (b) the wave function is continuous for all radii**; furthermore, their calculation neglected spin, spin-orbit and spin-spin effects, and Lamb shift, which are significant effects at small radius. Therefore, we consider their work as an interesting hint but not the proof. As we will see later, one needs to add a stronger attractive potential at small radius to make such atom stable (all potentials shown of Fig. 3b. That makes the math more complicated to solve. Instead, we will provide a simpler approach to the problem in the next chapters.

We should point out that an alternative theory to [4,5] was also proposed by Deck et al. [13]. As we will see in chapter 1.5, Paillet and Meulenberg independently came to similar conclusions using V_{eff} potential. [21] Another simpler approach was made by M. Bednar, who calculated the problem assuming a simple hard ball potential simulating nucleus and Coulomb potential outside nucleus [14].

1.2. Solutions using the Virial theorem.

Virial theorem is important consideration to judge if the bound system is stable [15,16,17]. Virial relations can be used to draw conclusions on the dynamics of bound states without solving the equations of motion.

We use the following simple **iterative virial theorem procedure**, a relativistic equivalent of old 1D Bohr-like model [18]. The procedure to find solution is as follows: (a) electron's De Broglie wavelength is constrained by radius r through equation $\lambda = n2\pi r$ (n is integer, which defines integral number of wavelength in circumference), (b) electron momentum is determined from De Broglie equation $p = h/\lambda$ (from here one can calculate relativistic kinetic energy T_{kinetic} , β and γ), and (c) stable electron radius is determined by numerical method stepping through values of r until virial theorem is satisfied, which means a balance between electron relativistic kinetic energy and potential energy:⁴

$$T_{\text{kinetic}} = T_{\text{virial}} \quad (8)$$

where T_{virial} is expected kinetic energy, calculated from the total potential energy U as follows:

$$T_{\text{kinetic}} = \sqrt{(hc/\lambda)^2 + (mc^2)^2} - mc^2 \quad (9)$$

where $\lambda = (2\pi/n)$ is De Broglie wavelength for electron radius r , and n is number of wavelength periods. Virial theorem states that for a general potential energy $V(r) = \alpha r^k$, the expected electron kinetic energy T_{virial} is related to potential energy as:

$$T_{\text{virial}} = k [\gamma/(\gamma + 1)] U, \text{ where } \gamma = 1/\sqrt{1 - (v/c)^2} \quad (10)$$

For example, for Coulomb potential ($U_1 = -k_1/r$), $k = -1$, and the kinetic virial energy is behaving as $T_{\text{virial}} \rightarrow -(1/2)U_1$ as $\gamma \rightarrow 1$, and as $T_{\text{virial}} \rightarrow U_1$ as $\gamma \rightarrow \infty$.

This method is basically a potential-based numerical iterative search for a solution of equation (8) by varying radius, while constraining De Broglie wavelength. This does not represent a real solution of quantum mechanical equations, but the method, we believe, gives a good approximation.

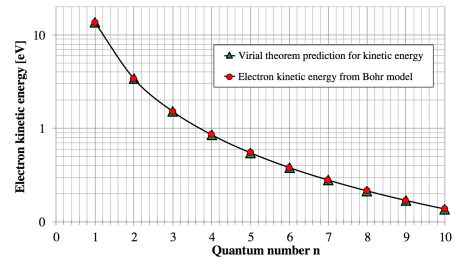


Figure 4 In normal hydrogen atom electron kinetic energy balances with potential energy according to virial theorem.

What is the meaning of radius r in various equations? Radius in relativistic Schrödinger or Dirac equations is mapping probability where electron is located. Similarly, in our simple iterative virial theorem model, we consider radius r_{stable} , as a variable to constrain the De Broglie wavelength length, which in turn defines the frequency of oscillation.

⁴ Reference [18] three methods to apply virial theorem to this problem. All three methods agree.

1.3. Virial theorem with Coulomb potential

If one applies equations (8) to the normal hydrogen atom using the Coulomb potential, electrons on all orbits satisfy the virial theorem, as shown on Figure 4.

However, if one applies equations (8) to the small hydrogen, one finds that the Coulomb potential alone is unable to hold electron on a stable deep orbit, i.e., the virial theorem is violated. This is illustrated on Fig. 5, which shows that only a solution for normal hydrogen exists. This is also true if we add either Smith-Johnson or Nix potentials to Coulomb potential. We need to use stronger force, as is discussed in the next few chapters.

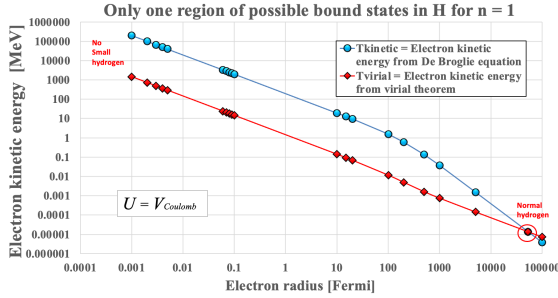


Figure 5 There is only one region of stability for Coulomb potential in the e-p system, corresponding to the normal hydrogen. The small hydrogen cannot exist with this potential.

1.4. Virial theorem with $V_{(Spin.B)}$ potential.

We assume that the attractive potential is dominated by a sum of two terms, the Coulomb potential $V_{Coulomb}$ and the Dirac spin-orbit term $V_{(Spin.B)}$; both potentials are already used for the normal hydrogen, $V_{Coulomb} = -KZe^2/r$ explains its stability, and $V_{(Spin.B)}$ potential explains the hyperfine spectral structure, which is a tiny effect for electron at large radius, but near proton it dominates. We assume that the spin-orbit potential energy is:

$$V_{(Spin.B)} \sim -g \mu_0 B, \quad (11)$$

where $\mu_0 = 5.788 \times 10^{-9}$ eV/Gauss is the Bohr magneton, $g = 2.0023$, B is electron "self-induced" magnetic field. To understand the origin of this magnetic field, we shall assume a simple equivalent model, where the electron is considered to be at rest and the proton is moving around at this radius.⁵ One can estimate the magnetic field value as follows:

$$B \sim 10^{-7} 2 \pi I / r = 10^{-7} Z e v / r^2 \quad (12)$$

where I is the circular loop current, Z is atomic number and v is electron velocity. Magnetic field is extremely high, calculated using equation (12) at very small distance from proton. To understand the origin of this magnetic field, we shall assume a simple equivalent model, where the electron can be considered to be at rest and the proton is moving around at this radius. Such electron is subject to a very high magnetic field of $B \sim 5.95 \times 10^{15}$ Gauss at radius of ~ 2.84 Fermi, making the spin term in equation (12) dominant and equal to $V_{(Spin.B)} \sim 69.04$ MeV, while the Coulomb energy contribution to the balance is only ~ 0.5075 MeV at the same radius.

⁵ Such calculation is used in many text books. For example, P.A. Tipler [5] used a similar approach to calculate the spin-orbit fine-structure splitting of spectral

Figure 6 demonstrates that adding a potential $V_{(Spin.B)}$ to Coulomb potential, virial theorem is satisfied at $r \sim 2.84$ Fermi and a stable small hydrogen is allowed. Table 3 shows deep levels where small hydrogen is stable for several n values. We can see that the mass of small hydrogen $M(pe^-)$ is ~ 938.276 MeV and binding energy $E_{BE} \sim -507.5$ keV.

The small hydrogen cannot be formed spontaneously since electron can obtain only ~ 0.5075 MeV at radius of 2.84 Fermi from the available static Coulomb potential energy. This means that the energy has to be supplied to electron externally to form the small hydrogen (in this respect it is similar to the electron capture on proton ($p + e^- \rightarrow n + \nu_e$), which requires external of > 0.708 MeV.

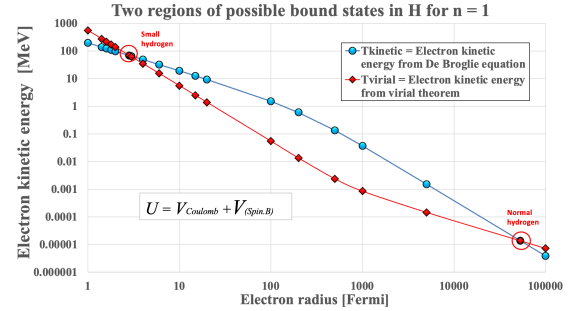


Figure 6 Two regions of hydrogen atom stability for a choice of potential of $V_{Coulomb} + V_{(Spin.B)}$ for $n = 1$.

Table 3 – pe^- small hydrogen:

$U = V_{Coulomb} + V_{(Spin.B)}$:

n	r_{stable} [Fermi]	$V_{(Spin.B)}$ [MeV]	$U = V_{Coulomb} + V_{(Spin.B)}$ [MeV]	$T_{kinetic}$ energy [MeV]	$M(pe^-)$ mass* [MeV/c ²]	E_{BE}^{**} [keV]
1	2.838	-69.04	-69.547	69.04	938.276	-507.5
2	1.4136	-278.201	-279.220	278.709	938.271	-511.7
3	0.94078	-628.115	-629.645	629.135	938.272	-510.9

* Mass of small hydrogen: $M(pe^-) = m_{proton} + \gamma m_{electron} - |U|$
 $m_{neutron} = 939.565413$ MeV/c², $m_{proton} = 938.272088$ MeV/c²

** Binding energy: $E_{BE} = T_{kinetic} - |U|$

1.5. Virial theorem with V_{eff} potential

Paillet and Meulenberg [21,22,23] independently concluded that small hydrogen may exist. They used the Heisenberg uncertainty principle (HUR) to estimate electron momentum if it is constrained to radius r . The HUR can be expressed by the well-known inequality $\Delta p \Delta x \geq \hbar/2$. From there authors estimated the average momentum of $p \sim \hbar / \langle r \rangle$. Adamenko and Vysotskii [24] proved, using Dirac equation, that the effective potential energy V_{eff} determining movement of relativistic electron in Coulomb field follows this equation:

$$V_{eff} = \gamma V_{Coulomb} + V_{Coulomb}^2 / 2mc^2 \quad (13)$$

Paillet and Meulenberg used this potential and obtained a stable orbit at small radius. To find a stable solution, Paillet and Meulenberg developed analytical method searching for a local minimum of electron energy in a combination of potentials near the nucleus. After the minimum was found, the virial theorem was checked.

lines in the normal hydrogen atom, where he obtains the self-induced magnetic field of $B \sim 4 \times 10^{13}$ Gauss at $r \sim 2.12 \text{ \AA}$.

In this paper, I confirm the results of Paillet and Meulenberg that the small hydrogen is stable with V_{eff} potential, however, this time using my iterative method proposed in this paper; my result is shown on Fig.7 and in Table 4. One can see that for large values of n , the binding energy approaches 511 keV.

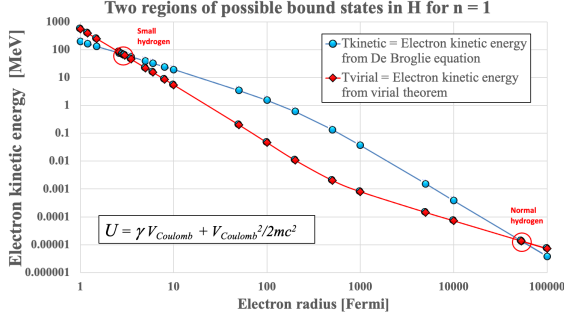


Figure 7 Two regions of hydrogen atom stability, one for normal hydrogen and one for the small hydrogen, calculated for potential energy $V_{eff} = \gamma V_{Coulomb} + V_{Coulomb}^2/2mc^2$ for $n = 1$.

Table 4 – pe^- small hydrogen:

$$V_{eff} = \gamma V_{Coulomb} + V_{Coulomb}^2/2mc^2:$$

n	r_{stable} [Fermi]	$U = \gamma V_{Coulomb} + V_{Coulomb}^2/2mc^2$ [MeV]	$T_{kinetic}$ [MeV]	$M(pe^-)^*$ mass [MeV/c ²]	E_{BE}^{**} [keV]
1	2.8284	-69.812	69.302	938.274	-508.6
2	2.8232	-139.881	139.370	938.273	-510.0
3	2.8214	-209.949	209.438	938.272	-510.6
1000	2.81802	-70067.72	70067.21	938.272	-511.0

* Mass of small hydrogen: $M(pe^-) = m_{proton} + \gamma m_{electron} - |U|$
 $m_{neutron} = 939.565413 \text{ MeV}/c^2$, $m_{proton} = 938.272088 \text{ MeV}/c^2$
 $m_{proton} + m_{electron} = 938.7830969461$

** Binding energy: $E_{BE} = T_{kinetic} - |U|$.

Tables 3 and 4 show that small hydrogen is stable, based on argument that $M(pe^-) < m_{proton} + m_{electron}$. Notice also that binding energy E_{BE} values in these tables are close to E_{DDL} values shown in Table 2b, obtained using completely different calculation. Another interesting conclusion is that mass of small hydrogen $M(pe^-)$ is slightly smaller than mass of neutron.

If this simple iterative model with this or similar potential describes the small hydrogen reality the small hydrogen will remain at $n = 1$ state, as any excitation requires too much increase in electron kinetic energy. **The small hydrogen will appear “dark” for outside observer.**

Table 5 – e^+e^- small positronium:

$$V_{eff} = \gamma V_{Coulomb} + V_{Coulomb}^2/2mc^2:$$

n	r_{stable} [Fermi]	$V_{eff} = -\gamma V_{Coulomb} + V_{Coulomb}^2/2mc^2$ [MeV]	$T_{kinetic}$ [MeV]	$M(e^+e^-)^*$ mass [MeV/c ²]	E_{BE}^{**} [MeV]
1	5.647	-34.966	34.713	1.024	-0.253

* $M_{e^+e^-} = m_e + m_e + \gamma m_{reduced} - |U|$

** Binding energy: $E_{BE} = T_{kinetic} - |U|$

$m_{electron} = 0.5109989461$, $m_{electron} + m_{electron} = 1.021997892$

We can apply our iterative method even for other small atomic systems, such as small positronium (e^+e^-), as shown on Fig.8 and in Table 5. One can see that E_{BE} in Table 5 is rather close to result in Table 2c, obtained using a different method. Table 5 also shows that small e^+e^- positronium atom is unstable because $M(e^+e^-) > m_{e^+} + m_{e^-}$. From the same reason, we find

that small muonium is also unstable. Figure 8 also shows a solution for normal positronium with radius of 106000 Fermi and mass of 1.02198 MeV; this state is presently accepted by QED and it is also unstable.

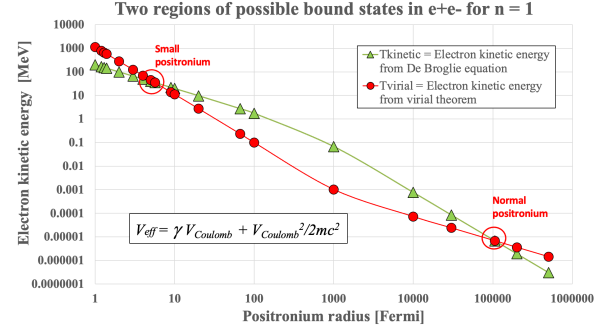


Figure 8 Two regions stability for positronium (e^+e^-). Calculated for potential energy $U = \gamma V_{Coulomb} + V_{Coulomb}^2/2mc^2$.

1.6. Virial theorem with V_{Yukawa} potential

Yukawa [25] in 1932 proposed this form of potential energy, to explain an exchange of a virtual particle of mass m between two fermions inside nucleus:

$$V_{Yukawa} = (A/r) e^{-Bmr} \quad (13)$$

where A is magnitude scaling constant, m is mass of virtual exchanging particle, r is radial distance to the particle, and B another scaling constant which have specific dimensions, and $r \sim 1/(Bm)$ is the approximate range of the potential. If mass m is zero, eq.(7) reduces to $V_{Coulomb} = A/r = -Ke^2/r$. Applying the Yukawa potential to our problem, we assume that exchanging virtual particle between relativistic electron and proton is a virtual photon with a non-zero mass. Experimental limit of photon mass is $\sim 7 \times 10^{-17} \text{ eV}$. In this section of the paper, we make an **ansatz** that photon develops a non-zero mass while interacting with nuclear medium, a physics which is yet to be proven.

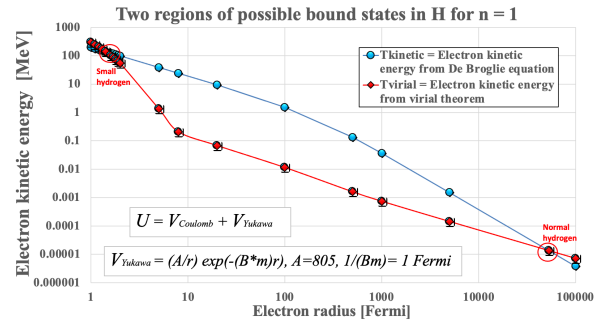


Figure 9 Two regions of hydrogen atom stability for $n = 1$, one for normal hydrogen and one for the small hydrogen; calculated for $A = 805$, $1/(Bm) = 1 \text{ Fermi}$.

Figure 9 and Table 6 show an example, where parameters were selected, presently arbitrarily, to demonstrate that the Yukawa potential can also hold electron on a stable orbit in small hydrogen. As one increases the potential range $\sim 1/(Bm)$, a stable radius r_{stable} increases, E_{BE} decreases and electron kinetic energy $T_{kinetic}$ decreases and mass of virtual exchanging

photon decreases; Table 6 shows that mass of small hydrogen remain about constant.

Table 6 – pe^- small hydrogen:

$$U = V_{Coulomb} + V_{Yukawa}:$$

(vary $1/(Bm)$, for $A=805$, $n=1$):

$1/(Bm)$ [Fermi]	r_{stable} [Fermi]	V_{Yukawa} [MeV]	$U=V_{Coulomb}+V_{Yukawa}$ [MeV]	$T_{kinetic}$ [MeV]	$M(pe^-)$ mass* [MeV/c ²]	E_{BE}^{**} [keV]
0.5	0.706	-277.51	-279.545	279.03	938.273	-510.2
1	1.413	-138.74	-139.772	139.26	938.273	-510.0
1.5	2.119	-92.50	-93.178	92.67	938.275	-507.6
2	2.825	-69.376	-69.886	69.38	938.274	-508.9
5	7.064	-27.743	-27.947	27.445	938.281	-501.8
10	14.133	-13.860	-13.961	13.469	938.291	-492.4

* Mass of small hydrogen: $M(pe^-) = m_{small\ hydrogen} = m_{proton} + \gamma m_{electron} - |U|$

$m_{neutron} = 939.565413\text{ MeV}/c^2$, $m_{proton} = 938.272088\text{ MeV}/c^2$

$m_{proton} + m_{electron} = 938.7830969461$

** Binding energy: $E_{BE} = T_{kinetic\ energy} - |U|$.

One can also apply this methodology to ϕ -meson, which is ss-bar quark bound system. We will use the Yukawa potential. Radial distances are much smaller in this case, a fraction of Fermi. Table 7 and Fig.10 shows that we can come up with a stable orbit at $r \sim 0.243$ Fermi for Yukawa parameters of $A = 1000$ and potential range of $1/(Bm) \sim 0.15$ Fermi. The ϕ -meson mass is very sensitive to a choice of potential range parameter.

Table 7 – $\phi = ss\text{-bar}$:

$$U = V_{Coulomb} + V_{Yukawa}:$$

($1/(Bm) \sim 0.1452$, for $A=1000$, $n=1$):

$1/(Bm)$ [Fermi]	r_{stable} [Fermi]	V_{Yukawa} [MeV]	$U=V_{Coulomb}+V_{Yukawa}$ [MeV]	$T_{kinetic}$ [MeV]	$M(\phi)$ mass* [MeV/c ²]
0.1452	0.2405	-793.5	-794.17	279.03	1020.09

* $M_{\phi\text{-meson}} = m_s + m_{s\text{-bar}} + \gamma m_{reduced\ mass} - |U|$

Mass of s-quark $M_s = M_{s\text{-bar}} = 92\text{-}104 \sim 100\text{ MeV}/c^2$

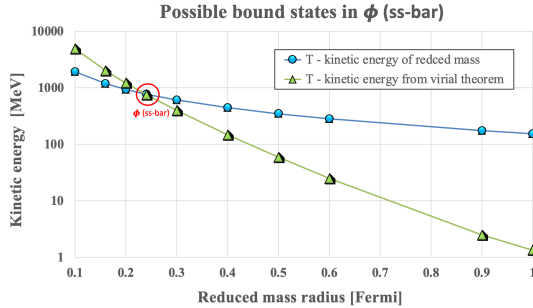


Figure 10 One region of ss-bar stability for $n = 1$, where virial theorem is satisfied; calculated for $A = 1000$, $1/(Bm) = 0.1452$ Fermi.

Our predicted value is close to measured value of $1019.461 \pm 0.020\text{ MeV}/c^2$. We predict that it is unstable because $M(\phi) > M_s + M_{s\text{-bar}}$; indeed, the ϕ -meson measured mean lifetime of $1.55 \pm 0.01 \times 10^{-22}\text{ s}$.

1.7. Potentials and kinetic energy.

It is useful to present various potentials used in this paper. Figure 11 shows radial dependency of absolute value of potential energies of $V_{Coulomb}$, V_{eff} , $V_{(Spin.B)}$, V_{Yukawa} and their relationship to electron kinetic energy, $\beta = v/c$ and γ . One can see that the problem becomes relativistic for $r < 500$ Fermi, where electron's γ starts increasing and $\beta = v/c$ approaches 1. The Coulomb potential contribution dominates for $r > 1000$

Fermi for all “small radius”-potential choices, which act as a small perturbation in normal hydrogen.

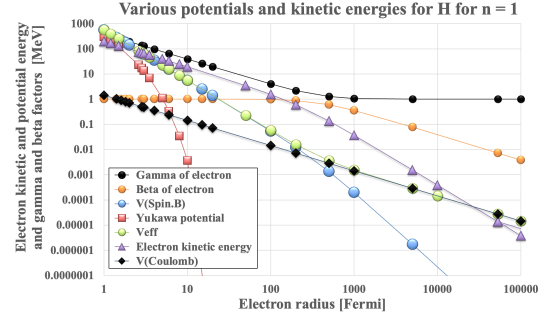


Figure 11 Comparison of potential energies V_{eff} , $V_{(Spin.B)}$, $V_{Coulomb}$, V_{Yukawa} , and electron kinetic energy $T_{kinetic}$ and for the “ $n = 1$ solution”, where $n = (2\pi r/\lambda)$, and λ is electron De Broglie wavelength; graph also shows electron γ -factor and β as a function of electron radius.

2. Expected interactions of small hydrogen

We will assume that the small hydrogen interactions are to large degree similar to neutron interactions. At large energies, small hydrogen will cause neutron-like hadronic showers. At small energies there may be some difference. From a distance of $>10\text{-}20$ Fermi, it will act as a neutron. However, from a distance of a 1-2 Fermi from nucleus, it will act as a small dipole electric moment and may not easily enter nucleus at very low energies. One would expect that its nuclear capture cross-section will be smaller than neutron nuclear capture cross-section. If it happens the nuclear capture of small hydrogen may destabilize nucleus to create emission of β , γ , α , γ particles and various nuclear fragments.

In a gaseous medium, the energy deposit (dE/dx) of small hydrogen is approximately 10^7 times smaller than that of a typical charged particle.

Small hydrogen is not ionized through collisions with light nuclei or other small hydrogen atoms, even at high velocities typical of cosmic phenomena. For instance, in the Bullet Cluster galaxy collision, with a velocity of 4500 km/s (corresponding to a kinetic energy of $\sim 105\text{ keV}$ for small hydrogen), ionization of small hydrogen remains unlikely – see Fig.20.

If energy exceeds $\sim 511\text{ keV}$, ionization of small hydrogen becomes possible. At significantly higher energies, small hydrogen behaves similarly to a neutron, capable of initiating a hadronic shower. At small or thermal velocities, small hydrogen could be captured by nuclei and participate in nuclear reactions.

3. Direct detection of small hydrogen

3.1. Formation of normal hydrogen

A free thermal electron, when approaching thermal proton, it is captured on highest level first, and subsequently gains total energy of $\sim 13.6\text{ eV}$ from available electrostatic potential energy and latches on the ground level with a correct De Broglie wavelength, where electron has a radius $r \sim 0.529\text{ \AA}$ and De Broglie wavelength of $\lambda \sim 3.222\text{ \AA}$, which corresponds to electron kinetic energy of $E_{kinetic} \sim 13.6\text{ eV}$ (it is balanced with potential energy as required by the virial theorem). If there is a large mismatch in energies of electron and proton, they will not form the normal hydrogen.

3.2. Proposed accelerator test to find small hydrogen

We will use the same argument for the small hydrogen. Table 4 tells us that electron radius is ~ 2.828 Fermi, the DeBroglie wavelength is ~ 17.762 Fermi, electron kinetic energy is ~ 69.302 MeV and v/c is ~ 0.999973212 . Ideally, for maximum efficiency, proton should have the same velocity as electron, which corresponds to proton total energy of 128.189 GeV. Electron and proton are then not moving together and can combine to form a stable small hydrogen because electron has right wavelength to latch. This means that to form the small hydrogen one requires two high energy accelerators.

Table 8 - Electron and proton kinetic energies needed to form small hydrogen in flight (both particles have the same $\beta = v/c = 0.9999732$):

Potential	Electron kinetic energy [MeV]	Proton kinetic energy [GeV]
V_{eff}	69.301	128.189

I suggest to send electrons and protons in the same direction, as shown on Fig.12a. The required beam kinetic energies are shown in Table 8. The gamma detector is placed at $\phi = 6.9^\circ$. If the small hydrogen atom is formed, a ~ 508.6 keV gamma in the two-particle rest frame. In the lab frame, the photon energy is very sensitive to the choice of ϕ angle due to the Doppler effect. The ϕ angle is angle between the direction of motion and gamma detector position:

$$E_{\text{Observed}} = E_{\text{Source}} / [\gamma (1 - \beta \cos \phi)] \quad (14)$$

Figure 12b shows this dependency on the angle ϕ , based on equation (14). The gamma detector should be positioned at $\phi \sim 6.9^\circ$ to measure $E_{\text{Observed}} / E_{\text{Source}} \sim 1$. Energy of gammas produced at $\phi = 0^\circ$ will be boosted from 0.5086 MeV to 138.9 MeV. In this case, one will detect gamma and hadronic shower well separated.

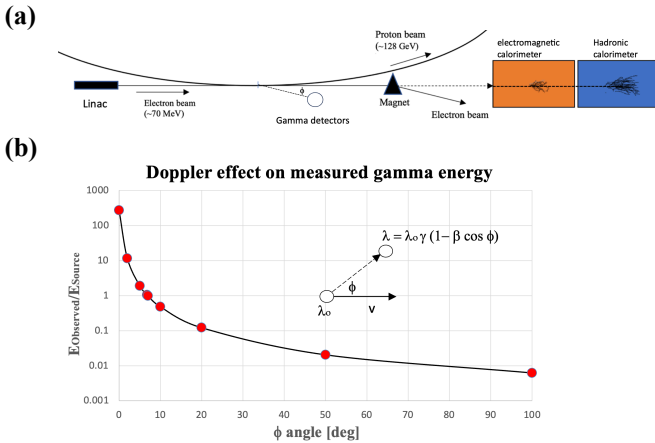


Figure 12 (a) Schematic concept to prove that the small hydrogen exists. Proton beam is brought tangentially to electron beam so that both beams travel parallel to each other for some distance. If the small hydrogen is formed, it will emit a 508.6 keV gamma in the two-particle rest frame, while electrons are deflected by a magnet. (b) Gamma energy is boosted due to the Doppler effect to high values at very forward direction from a source traveling at velocities close to velocity of light – see equation (14).

There are two possibilities of detection: (a) the gamma goes to gamma detector located at $\phi = 6.9^\circ$, and the small hydrogen makes a large shower in the hadronic calorimeter, or (b) the gamma produced at $\phi \sim 0^\circ$ would create a large electromagnetic in electromagnetic calorimeter and the small hydrogen will create a large collinear hadronic shower in the hadronic calorimeter, both well separated in space, but not in time. The idea is to tune beam energies and observe a peak at expected electron and proton energies. **This result would be a direct proof of small hydrogen existence. This measurement is a high energy physics equivalent to what were the 1920's bench-top experiments.**

At present, the only places where such experiment is feasible are Brookhaven National Lab (BNL), Fermilab or CERN (protons of ~ 128.2 GeV already exist at the CERN SPS and a ~ 69.3 MeV electron accelerator may not be that difficult to construct).

3.3. Search for small hydrogen in high energy collisions

Figure 13 suggests a test, which could be performed in large high energy experiments such as BaBar [34], Belle-II, LHCb, CMS, ATLAS, or Electron-ion collider (EIC). LHCb with its excellent electron and proton identification and high momentum reach is especially suitable for this search as momenta shown in Table 9 can be easily reached. Aim is to search for a neutral particle with mass close to neutron mass. Initially two independent particles, electron and proton, would form ep-bound state, probably accompanied by a ~ 0.5 MeV gamma emission (in their rest frame). There are three possibilities: (a) it will leave the detector as a missing mass, if a stable e-p bound state is produced (this is usually hard to prove in very complicated events, and in LHCb, since it does not have a 4π coverage); (b) there will be no secondary decay vertex, if lifetime is extremely short; (c) one may detect and observe a V-decay in vertex chamber, if lifetime is within a detectable range.

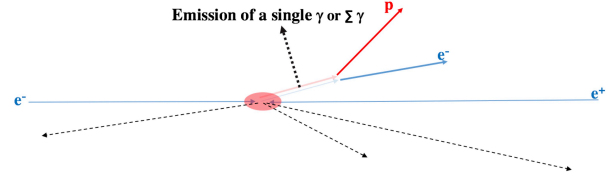


Figure 13 Proposal to search for e-p bound state in BaBar, Belle-II or LHCb data. It will show up as a peak in the e-p effective mass distribution close to mass of the small hydrogen.⁶

3.4. Schott's equivalent model of hydrogen

We would like to mention this model, which is now outdated, but nevertheless useful to introduce the next chapter. How Schott would view the small hydrogen? Schott [26] has demonstrated in 1933 that a uniformly charged spherical shell of radius r , undergoing periodic orbital motion of period T , does not radiate provided the shell radius is an integral multiple of $cT/2$, where c is the speed of light; **the orbit need not be circular nor even planar, it can be a vibration in 3D**. Other people verified the Schott's idea mathematically [27,28,29]. For example, for a choice of potential according to Table 4, $r_{\text{stable}} \sim 2.828$ Fermi, and proton is surrounded by “standing

⁶ A brief preliminary analysis of the BaBar data was attempted by Matt Bellis; it was not finished due to difficulty with large background near expected small

hydrogen mass of ~ 938.27 MeV/ c^2 ; one should return to it with more sophisticated analysis.

electron wave” with the De Broglie wavelength of 17.75984 Fermi and oscillating with very high frequency of $\sim 1.688 \times 10^{22}$ Hz. That is a very high number, but applying the same idea to the normal hydrogen, the Schott’s frequency of electron wave is $\sim 9.03 \times 10^{17}$ Hz, still a very large number. In this 1D picture, the small hydrogen is just a different hydrogen atom with electron oscillating at higher frequency. If we accept this 2D or 3D view of small hydrogen, we may have to deal with two or three quantum numbers.⁷

3.5. Can the small hydrogen be formed during the plasma oscillations in core of stars ?

Chapter 3.4 suggests that in small hydrogen proton is surrounded by a “standing electron wave” oscillating at very high frequency of $\sim 1.688 \times 10^{22}$ Hz. While this value is remarkably high, the equivalent equivalent frequency for normal hydrogen is $\sim 6.6 \times 10^{15}$ Hz, also significant value.

This raises the intriguing possibility that small hydrogen could form during plasma oscillations, where electrons coherently oscillate relative to relatively stable nucleons. We propose that if the electron plasma frequency approaches values dictated by de Broglie’s model, small hydrogen formation becomes feasible. To achieve a plasma frequency of $f_e \sim 10^{22}$ Hz, the required electron plasma density is approximately $n_e \sim 10^{35} \text{ cm}^{-3}$. The oscillation frequency is given by [12]:

$$f_e \sim (e^2 n_e / \epsilon_0 m_e)^{1/2} / 2\pi \quad (15)$$

where e is the electric charge, n_e is electron density, ϵ_0 permittivity of vacuum and m_e is the electron mass. Table 9 shows examples of plasma parameters for various plasma densities⁸.

Currently, achieving such high densities in Earth-based laboratory conditions appears impossible. The highest densities obtained, such as in laser fusion, remain insufficient. However, during the collapse of massive stars into neutron stars, electron densities can reach $3.5 \times 10^{36} \text{ cm}^{-3}$, corresponding to a plasma frequency of $\sim 1.68 \times 10^{22}$ Hz, consistent with the electron wave frequency in small hydrogen.

As the inner core collapses to extremely high mass densities ($\sim 10^{14} \text{ g/cm}^3$) [15], electrons are forced into protons via inverse beta decay ($p + e^- \rightarrow n + \nu_e$). Gravitational pressure must supply at least **782.33 keV** to the electrons for this reaction to occur. During this collapse, outer layers compressed to densities of $\sim 1.25 \times 10^{13} \text{ g/cm}^3$ may allow conditions for small hydrogen formation. At densities exceeding $\sim 10^{11} \text{ g/cm}^3$, nucleons begin to “drop” out of nuclei [16].

Figure 14 illustrates the plasma frequency as a function of mass and electron density in a collapsing star, indicating the density region where neutron stars form and suggesting that slightly lower densities might permit small hydrogen formation.

Table 9 - Densities and temperature of typical plasma types

Type	Electron density [cm ⁻³]	Electron frequency [Hz]	Plasma temperature [keV]
The Sun’s core	$\sim 10^{22}$	$\sim 10^{15}$	2.3
Larger star	$\sim 10^{26}$	$\sim 10^{17}$	2
White dwarf	$< 6 \times 10^{31}$	$< 7 \times 10^{19}$	0.5-1.7
Supernova explosion which may produce the neutron star at center	$\sim 10^{40}$	$\sim 10^{24}$	8000-9000
Laser fusion [31]	$\sim 6 \times 10^{26}$	$\sim 2 \times 10^{17}$	2-3
Tokamac fusion	$\sim 10^{14}$	$\sim 2.8 \times 10^{11}$	10-20
Lightning in air	$\sim 10^{14}$	~ 100	< 0.01
Our sparking tests [32]	$< \sim 10^{17}$	$< \sim 3 \times 10^{12}$	< 10
Plasma near cathode in electrolysis [33]	$\sim 10^{13}$	$\sim 3 \times 10^{10}$	~ 0.0012

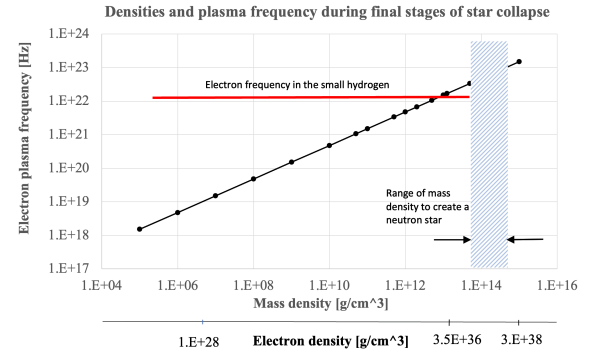


Figure 14 Plasma frequency as a function of mass and electron density during the collapse of a large star. The plot indicates the density region where neutron stars form, with slightly lower densities potentially allowing for small hydrogen formation.

If supernovae produce small hydrogen, the universe could contain a substantial population of these particles, resembling neutrons. Older galaxies with extended supernova activity may have a higher concentration of small hydrogen. Future experimental tests should focus on regions free from contamination by solar neutrons.

3.6. Search using large sparks in hydrogen gas

We attempted to detect **small hydrogen** in a tabletop experiment by generating large sparks in **hydrogen gas at low pressure**. These conditions created a small **pinch effect**, increasing the accelerating voltage enough to produce **10 keV X-rays**. A **1 mm spark gap** (Figure 15a) operated at **peak currents of 0.2–0.5 kA**, a **low pressure of ~ 2 Torr**, and a **spark gap electric gradient of ~ 25 kV/cm**. Each spark carried a total charge of more than 4×10^{14} electrons, with electron densities approaching $10^{17} \text{ electrons/cm}^3$.

Various detectors were used in these tests [32]: two back-to-back TPCs (Figure 15b), a photon-sensitive CsI-detector (Figure 16a), YAP-scintillator, gaseous wire tube chamber, and a neutron-sensitive BF₃-counter.

To identify the **small DDL hydrogen atom** in the laboratory, we aimed to observe either a clear 511 keV signal or a large shower of energetic gamma rays.

The total observed **X-ray energy per event** was typically over 100 keV per spark, consisting of many **2–10 keV X-rays**

⁷ Bohr-Sommerfeld model used two quantum numbers, radial and azimuthal.

⁸ Density in sparking tests [20] is likely to be higher than quoted in the table because of the pinch effect, which explains rather high X-ray energies observed.

(Figure 15c), calibrated using an Fe-55 source. X-rays were produced only when positive ions formed after electrons reached a sufficient energy threshold, creating a plasma. The plasma density may have reached $10^{17}/\text{cm}^3$ or higher, as indicated by the pinch effect producing **10 keV X-rays** at only **0.9–2.1 kV spark voltage**.

Figure 16b confirms that **no 511 keV gamma peak** was observed. However, a few events showed large energy deposits, along with multiple lower-energy X-rays per spark. No neutrons were detected in this test. One should add that the run lasted only an hour, so we cannot exclude a possibility of weaker signal. It may be beneficial to repeat such tests lasting much longer.

It may also be beneficial to repeat these tests at much higher voltages and currents, which could enhance the pinch effect and generate even higher accelerating voltages and plasma density.

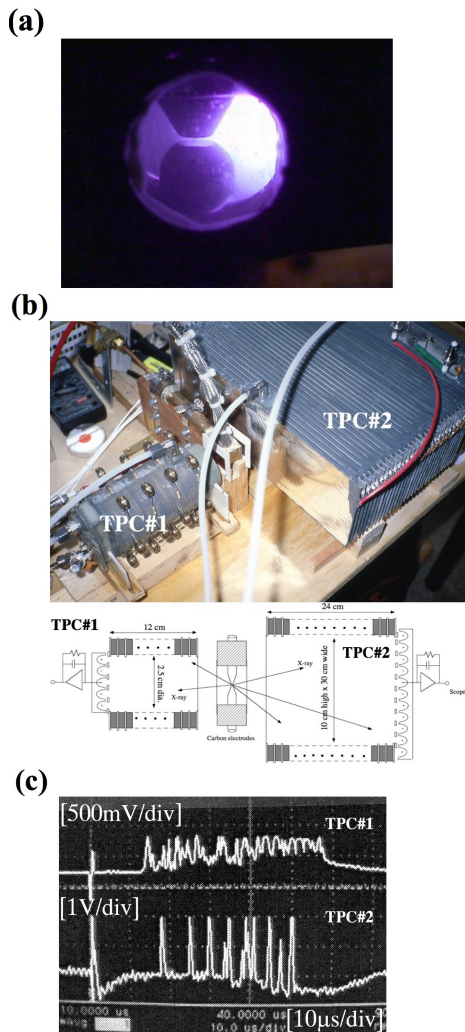


Figure 15 (a) Spark electrodes as viewed through Mylar window. (b) Two back-to-back TPCs. (c) Typical TPC pulses during a single spark. The total observed visible energy in our solid angle of all detected X-rays per event was typically 100-150keV/spark; a typical single event consists of many 2-10 keV X-ray pulses; the calibration was done by the Fe⁵⁵ source, which deposits ~5.9keV/pulse on average [32].

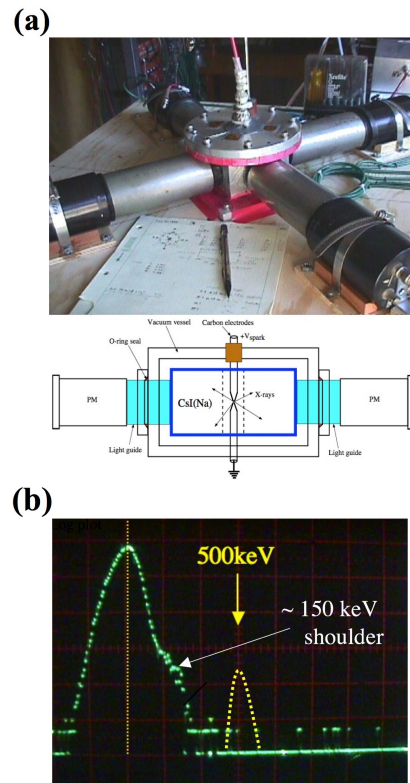


Figure 16 (a) Sparking tests by the author with the CsI crystal with a spark gap in the middle. (b) Again, one observes a hint of large energy deposit, although the precision was not very high in this test due to the sparking noise. The energy scale was calibrated by the Na²² source [32].

Thunderstorms and High-Energy Discharges: Usual atomic transitions in normal atoms produce single-photon emissions, typically explained using perturbation theory. However, since the energy difference between deep and normal levels in small hydrogen is much larger than in regular atoms, the usual perturbation methods may not apply. Instead, transitions might occur via multiple-photon emission, making it difficult to detect a distinct 511 keV peak. This idea was discussed with Nathan Isgur, who agreed with this possibility.

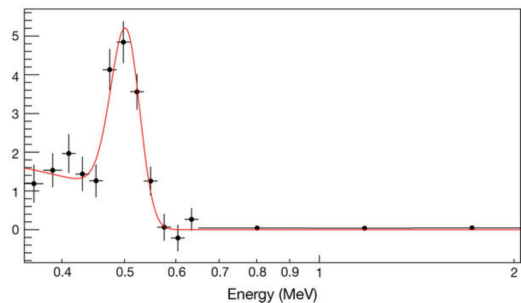


Figure 17 A prolonged ~0.511 MeV emission, which lasted for a minute, observed during the thunderstorm [35].

Thunderstorms and High-Energy Discharges: Figure 17 shows experimental evidence that thunderstorm lightning strikes produce high energy and high currents of electrons, positrons, ~0.511 MeV γ -rays, X-rays, and neutrons [35]. Most of lightning strikes reach currents of ~35 kA, charges up to ~20

Coulomb. These currents were two orders of magnitude larger than in our sparking tests on hydrogen gas [32].

References [36-38] explain this effect using atmospheric photonuclear reactions $^{14}\text{N} + \gamma \rightarrow ^{13}\text{N} + n$ and $^{16}\text{O} + \gamma \rightarrow ^{15}\text{O} + n$. These reactions generate fast neutrons (~ 10 MeV) and unstable radioactive isotopes, which undergo β^+ -decay, producing positrons responsible for the annihilation peak.

Although this is a likely explanation, the formation of small hydrogen could also be involved. Notably, results such as those in Figure 17 were the goal of our hydrogen sparking experiments (Figure 16b).

Since **thunderstorms are difficult to control**, A.V. Agafonov conducted **controlled discharge tests** in the lab using **air as a target** [39]. These experiments used (all these values are significantly larger than in our tests [32]):

- Sparking voltage ~ 1 MV
- Electric fields of ~ 10 kV/cm
- Currents of 10–12 kA

Resulting measured detected neutron fluxes were far **above expected rates**.

We suggest that the experiment incorporates a **hydrogen target** to see if it could still produce neutrons and a clear ~ 511 keV signal, which would be a signature of the small hydrogen formation.

3.7. Search using cosmic accelerators

One example of a cosmic accelerator is the jet of particle beams produced by **active galactic nuclei (AGN)**, which are powered by supermassive black holes. These jets, composed of radiation and particles, travel close to the speed of light and are aligned along the black hole's axis of rotation. A special class of AGN, known as **Blazars**, have their jets aimed directly at Earth. When observed from Earth, small hydrogen within these jets could possess extremely high energy.

Another example is **supernova remnant shocks**, which arise from the violent interactions of supersonic plasma. These interactions amplify magnetic fields and accelerate electrons and protons to highly relativistic speeds.

These sources could produce **small hydrogen with high energy**, which, upon interaction in a calorimeter, would generate **high-energy showers**. Detecting these showers would provide crucial insights into the properties of small hydrogen and its role in cosmic accelerators. Since neutrons would have decayed long ago, only stable small hydrogen could produce this signal.

Detecting **high-energy “neutron-like”** particle from these sources would require a **large hadronic calorimeter** optimized for high-energy particles. Additionally, the satellite observing these phenomena should be placed **far from the Sun and Earth** to minimize background contamination from these two sources.

3.8. The 511 keV signal from the center of our galaxy

One of the most intriguing puzzles in astrophysics is the origin of the **strong 511 ± 0.08 keV gamma signal** observed at the center of our Galaxy. Figure 18 shows this signal as detected by the **ESA INTEGRAL satellite observatory** [40].

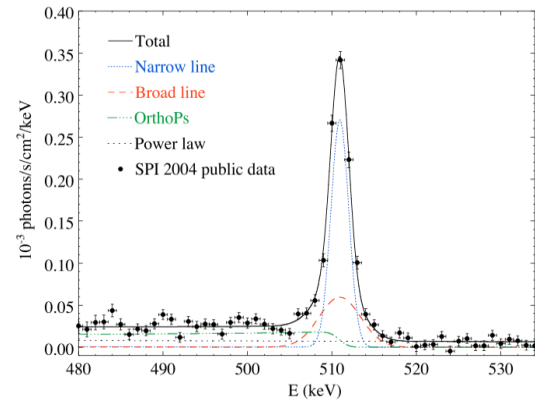


Figure 18 The 511 keV signal observed by the ESI instrument aboard the ESA Integral satellite observatory [40].

The most straightforward explanation for this signal is **electron-positron annihilation**. The observed spectrum can be well-described by a combination of annihilation emission, including narrow and broad Gaussian lines, an ortho-positronium continuum, and a power-law component accounting for Galactic diffuse emission. Calculations estimate a total **positron annihilation rate of $\sim 3 \times 10^{43}$ e⁺/sec**. The primary suspected sources of positrons are thermonuclear supernovae, where β^+ radioactive decay of isotopes such as ^{26}Al , ^{44}Ti , and ^{56}Co could produce the required positrons.

However, a significant challenge remains with this explanation. As noted in N. Prantzos's paper [40]:

"Despite 30 years of intense theoretical and observational investigation, the main sources of positrons have not been identified." More recent studies [41] confirm that there is no sufficient positron source to fully explain the observed 511 keV signal.

Due to the difficulty in identifying positron sources sufficient to explain the strength of this signal, numerous alternative hypotheses have been proposed. For example:

- **Dark matter annihilation** as suggested in Ref. [42].
- **Evaporating primordial black holes**, proposed in Ref. [43].

We propose an alternative explanation based on **small hydrogen**. As hydrogen gas is drawn into the supermassive black hole at the Galactic center, it becomes fully ionized, forming a **dense plasma**. Just before reaching the event horizon, **electrons may form deep orbits around co-moving protons**, emitting gamma photons near 510–511 keV (see Tables 2b, 3, 4, and 6).

3.9. Neutron capture in Integral satellite

Figure 19 presents an analysis of low-energy spectra, including nuclear capture signals, detected by the INTEGRAL satellite [40]. Since **INTEGRAL** is positioned in space where it **cannot detect thermal neutrons originating from the Sun**, the observed neutron capture peaks must have a different explanation. The most plausible hypothesis is that these peaks result from **cosmic-ray protons interacting with the satellite's structure**, producing secondary neutrons that are subsequently captured, leading to the emission of multi-MeV gamma rays. As noted in Ref. [40], this presents a puzzling issue: *"Thermal neutron capture is responsible for numerous and strong lines at several MeV, such as 2.223 MeV line; their*

unexpected presence poses a difficult challenge for our physical understanding of instrumental backgrounds and for Monte Carlo codes.”

The presence of **thermal small hydrogen** and its subsequent capture by nuclei could potentially explain these **previously unexplained** neutron capture signals. We propose an investigation into **thermal small hydrogen in outer space**. To achieve this, future missions should be placed **far from the Sun** and utilize **low-mass satellite structures** to minimize the production of thermal neutrons from cosmic proton interactions.

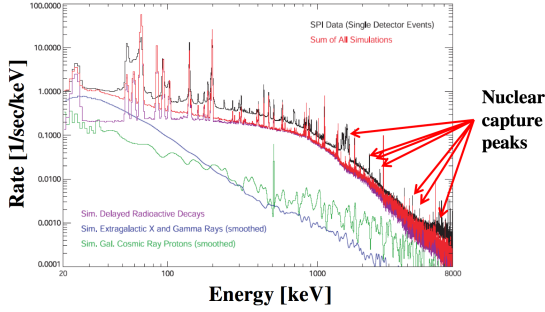


Figure 19 The thermal neutron capture signals detected by the Integral satellite [40]. This signal is not explained by their MC simulations.

3.10. Hyperfine structure of small hydrogen

The **hyperfine signal** plays a crucial role in astrophysics. A key question is whether **hyperfine splitting exists in small hydrogen**. In normal hydrogen, hyperfine splitting arises from the interaction between the proton’s magnetic dipole moment and the electron’s spin in the s-state. This effect is responsible for the well-known **21 cm line** observed in interstellar hydrogen, which results from an electron **spin-flip transition**.

For the ground-state of normal hydrogen, the spin-spin interaction potential for orbital quantum number $\ell = 0$ can be expressed as [47] (For now, we assume that the mathematical framework for the small hydrogen is the same as to the normal hydrogen):

$$\Delta E = E_{spin\ up} - E_{spin\ down} = \quad (15)$$

$$= \frac{8}{3} \mu_0 2.79 \mu_p \mu_e \frac{4}{h^2} \left(\frac{h^2}{4} - \frac{3h^2}{4} \right) \frac{1}{\pi r^3} = \frac{8}{3} \mu_0 2.79 \frac{eh}{2\gamma m_e} \frac{eh}{2m_p} \frac{1}{\pi a_0^3}$$

where $\mu_0 = 2\alpha h/e^2 c$ is vacuum permeability constant, $\alpha = 1/137$, γ is a relativistic gamma factor defined by eq.(10), $\mu_p = eh/2m_p$ is proton magnetic moment, $\mu_e = eh/2\gamma m_e$ is electron magnetic moment for the relativistic electron with relativistic mass γm_e , and a_0 is radius of electron where virial theorem is satisfied. As we see in equation (15), the electron magnetic moment is suppressed by γ -factor, which reduces the spin-spin effect for small hydrogen by a large factor [48].

For **normal hydrogen** atom, a stable radius is $a_0 = 52902$ Fermi and $\gamma = 1.000006669$, eq.(15) gives a value of $\Delta E = 5.87566 \times 10^{-6}$ eV for $z = 0$, which agrees with observation; it corresponds to famous **21.1 cm** wavelength line (or 1.4201 GHz frequency) observed in the Universe.

For **small hydrogen** atom, and stable radius is $a_0 = 2.828$ Fermi and $\gamma = 136.62$ (see Table 4), eq.(15) predicts a value of $\Delta E = 0.282276$ MeV for $z = 0$, which corresponds to wavelength of 4.3929×10^{-10} cm and frequency of 6.8048×10^{10}

GHz. We can see that the **spin effect is significant at small radius**.

Figure 20 shows small and normal hydrogen hyperfine signal from sources with red shift $z = 0$, $z = 10$ and $z = 1000$.

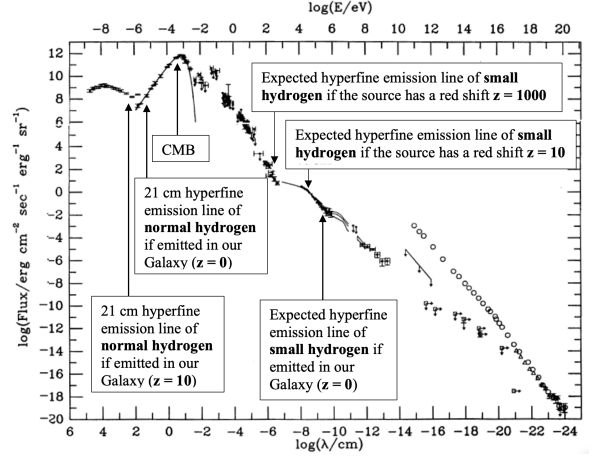


Figure 20 Flux of diffuse extra-galactic photons [49,50]. The cosmic microwave radiation (CMB) is clearly visible. We also show expected small and normal hydrogen hyperfine signal from sources with red shift $z = 0$, $z = 10$ and $z = 1000$.

One can ask what is significant about sources with $z = 10$. According to Ref.[51], the time around red shift of $z \sim 10$, only 500 million years after the Big Bang, represents a rapid galaxy build-up in the heart of the re-ionization epoch. Galaxies at that time increased both luminosity density and volume, perhaps providing enough energy for frequent spin flips of both small and normal hydrogen.

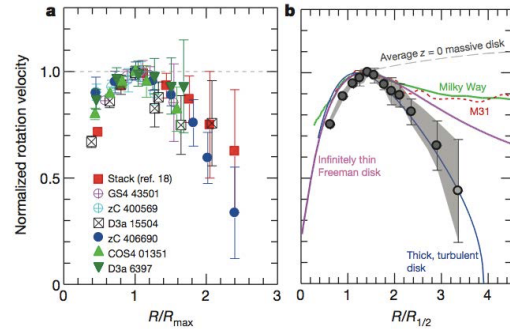


Figure 21 (a) Genzel’s paper [52] suggests that younger galaxies, located at $z = 0.6 - 2.6$, do not seem to have as much Dark Matter at large radii, resulting in a smaller rotation velocity at large radii. (b) Older local galaxies, located at $z = 0$, such as Milky Way or M31, do have a tail at large large radius (black points represent binned averages from figure (a)).

3.11. Young and old galaxies.

Figure 21 presents a recently published puzzle regarding dark matter distribution. Genzel et al. [52] suggest that younger galaxies (with redshifts $z = 0.6 - 2.6$) exhibit **lower dark matter content**, resulting in **smaller rotation velocities at large radii**. In contrast, **older local galaxies** ($z = 0$), such as the **Milky Way** and **M31 (Andromeda)**, show a **persistent tail of high rotation velocities at large radii**.

If confirmed with additional data, this finding could imply that the majority of dark matter is produced by the galaxy itself rather than being primordial. One possible explanation is that

small hydrogen is generated **within galaxies over time**, particularly through **supernova explosions**. Since **young galaxies** have not existed long enough to accumulate significant amounts of small hydrogen, their dark matter content—and consequently their rotation curves—would be lower compared to **older galaxies** that have undergone more supernova events.

4. Primordial small hydrogen?

Dark matter is **stable** and does not emit light or other radiation. One widely studied dark matter model, called **Cold Dark Matter (CDM)**, assumes that dark matter particles, called **WIMPs** interact only via gravity.

A more recent model, known as **Self-Interacting Dark Matter (SIDM)**, explains large-scale cosmic observations. This model proposes that dark matter particles interact not only gravitationally but also **among themselves with surprisingly strong interactions**. While the direct detection of dark matter would be groundbreaking, limits on SIDM can be inferred from cosmological observations, such as **galaxy cluster collisions** and **galaxy halo dynamics**.

Collisions between galaxy clusters, which contain dark matter, provide crucial tests for dark sector interactions. Reference [54] presents an up-to-date review of the status of SIDM model constraints. The predicted **self-interaction cross-section** starts at high values of $\sigma_{\text{DM}/m} \sim 5\text{--}30 \text{ cm}^2/\text{g}$ for very low velocities ($\sim 10\text{--}50 \text{ km/s}$) and appears to decrease as $\sim 1/v^4$ for velocities above a few hundred km/s [55].

For instance, in the well-known **Bullet Cluster**, dark matter is traveling at $\sim 1310 \text{ km/s}$, and SIDM analysis constrains its self-interaction cross-section to $\sigma_{\text{DM}/m} < 1.25 \text{ cm}^2/\text{g}$ [54]. Observations of **72 galaxy cluster collisions** using the **Chandra** and **Hubble Space Telescopes** have provided a statistical upper limit on the self-interaction cross-section: $\sigma_{\text{DM}/m} < 0.47 \text{ cm}^2/\text{g}$, although the authors did not specify the velocities involved.

Figure 22 illustrates the relationship between small hydrogen velocity and energy. At a velocity of $\sim 1310 \text{ km/s}$ (comparable to the Bullet Cluster), the small hydrogen particle would have a kinetic energy of approximately 10 keV (assuming $m_{\text{small hydrogen}} = 938.27 \text{ MeV}/c^2$).

Since this energy is insufficient to ionize small hydrogen atoms upon collision, their interactions would remain optically invisible, detectable only through gravitational effects.

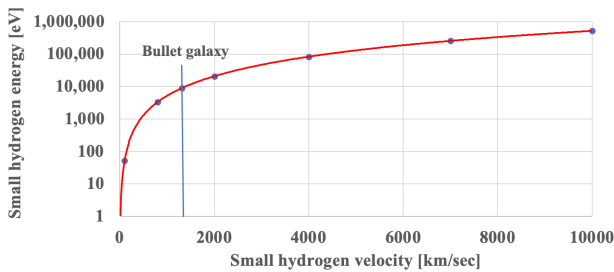


Figure 22 Relationship between small hydrogen velocity and energy. The Bullet galaxy velocity of $\sim 1310 \text{ km/sec}$ corresponds to small hydrogen kinetic energy of $\sim 10 \text{ keV}$.

In the absence of known cross-section values for small hydrogen scattering, we assume that neutron cross-sections

provide a reasonable approximation. Table 10 presents typical neutron scattering cross-sections for interactions with light nuclei at 10 keV neutron energy [56]. Figure 23 further shows that neutron cross-sections on light nuclei remain relatively stable between $\sim 0.1 \text{ eV}$ and $\sim 100 \text{ keV}$ [56].

For energies below $\sim 0.1 \text{ eV}$, neutron scattering cross-sections are **inversely proportional to velocity** and do not follow the $\sim 1/v^4$ decline preferred by SIDM models. This suggests that the values in **Table 10** may be somewhat **higher than those required for SIDM models** in interactions with light targets like **n, p, or He-4** ($6\text{--}12 \text{ cm}^2/\text{g}$). However, they could still be **consistent with SIDM models for heavier targets**, such as **Si** ($\sim 0.6 \text{ cm}^2/\text{g}$).

That said, even if small hydrogen exhibited **relatively large neutron-neutron cross-sections**, these interactions **would remain optically undetectable**. Much like dark matter, such particles could only be observed **gravitationally**, as demonstrated in Bullet Cluster collision analyses.

Table 10 – “Neutron-target nucleus” elastic scattering cross-sections for neutron incident energy of 10 keV [56]:

Collision of neutron with target nucleus	Cross-section [barns]	Cross-section [cm^2/g]
n	20.5	12.2
H ¹ (proton)	19.2	11.5
H ² (deuterium)	3.3	2.0
He ³ (tritium)	1.7	1.0
He ⁴	10.3	6.1
Li	1.1	0.7
C	4.8	2.9
O	3.8	2.3
Si	1	0.6
Ni	5.5	3.3
S	1	0.6
U ²³⁵	2.7	1.6

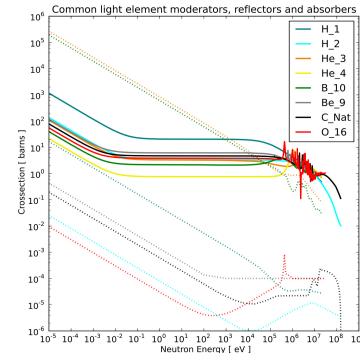


Figure 23 Scattering (full line) and absorption (dotted) cross-sections of neutron on light elements as a function of neutron energy [57,58].

6. LENR mechanism

LENR, or Low-Energy Nuclear Reaction, refers to a hypothesized type of nuclear reaction that occurs at or near room temperature—often referred to as “**cold fusion**.” We refer here to a recent review paper [58], which summarizes the current state of the field and attempts to explain LENR using known physics. It concludes that enhancements of up to **40 orders of magnitude** over the baseline spontaneous fusion rate of deuterium gas could potentially be achieved (with deuterium embedded in a **palladium (Pd) crystalline structure**).

Although this quoted increase is impressive, it is still not sufficient to make the cold fusion rate practically significant.

Based on what has been discussed in the previous sections, it would seem impossible to create **small hydrogen** under typical “cold fusion” experimental conditions. However, we acknowledge that we are not fully familiar with all the intricacies of solid-state physics or the specific experimental conditions used in these tests.

One possible approach could involve irradiating **Pd-D** or **Pd-H** samples with **gamma rays of appropriately chosen energy** to investigate whether ejected electrons could be captured into deep energy levels. The **flux, energy, or type of incident irradiation** would need to be carefully tuned. Once **small hydrogen** or **small deuterium** is formed, fusion rates in these crystals are expected to increase.

Conclusions

This paper argues that studying small hydrogen is a valuable pursuit, both theoretically and experimentally.

We have shown that the Coulomb potential alone is insufficient to bind an electron at deep energy levels. Instead, an additional, stronger potential - such as the (Spin.B) force - must be considered. While this force is weak in normal hydrogen, where it causes hyperfine splitting, it becomes significantly stronger at small radii, enabling the formation of small hydrogen

Furthermore, the Coulomb potential does not provide enough energy for an electron to transition spontaneously to deep levels. Instead, external energy input is required, much like electron capture on a proton. This suggests that small hydrogen can only form in extreme environments, such as high-energy physics experiments or supernova explosions, rather than spontaneously. This constraint explains the stability of ordinary matter.

We propose that the observed 511 keV gamma-ray signal from the center of our Galaxy may result from transitions involving small hydrogen.

Several high-energy physics and astrophysics experiments have been suggested as potential methods for detecting small hydrogen, as simple tabletop experiments are unlikely to suffice

If small hydrogen is indeed produced in supernovae, it could help explain differences in rotational velocity distributions between young and old galaxies. Additionally, it may provide insight into the Bullet Cluster collision, as small hydrogen would be optically “dark” at high velocities while remaining detectable through gravitational effects.

The most critical next step is to find experimental evidence for small hydrogen. A more refined theoretical framework will follow once its existence is confirmed.

Acknowledgements

I would like to thank J. Bjorken, S. Brodsky, J. Vary, J. Jaros, M. Bednar, R. Forty, N. Isgur and R. Wagoner for useful comments; especially to Stan Brodsky for critical comments of original calculation using Klein-Gordon and Dirac equations. I also thank to Tom Abel for suggesting SIDM models. Discussions with J.L.Paillet and A. Meulenberg are also appreciated.

References

- [1] R. Reeves, “A force of Nature”, page 114, Atlas books, New York - London, 2008.
- [2] A. Pais, “Inward bound”, page 397, Clarendon press - Oxford, 1986.
- [3] L. I. Schiff, “Quantum Mechanics”, (equation 53.16, page 470), 3rd ed., McGraw-Hill Publishing Company, New York (1968).
- [4] J. Maly and J. Va’vra, “Electron Transitions on Deep Dirac Levels I”, Fusion Technology, Vol. 24, November 1993.
- [5] J. Maly and J. Va’vra, “Electron Transitions on Deep Dirac Levels II”, Fusion Technology, Vol. 27, January 1995.
- [6] J. Va’vra, “On a possibility of existence of new atomic levels, which were neglected”, Nov.25, 1998 Siegen Univ., Germany
https://www.slac.stanford.edu/~jjv/activity/DDL/1_st_talk_siegen.pdf
- [7] F.C. Smith and W.R. Johnson, “Relativistic Self-Consistent Fields with Exchange”, Phys. Rev. 160, 136–142 (1967).
- [8] B.W. Bush, J.R. Nix, Ann. of Phys., 227, 97 (1993).
- [9] E.E. Salpeter and H. Bethe, “A Relativistic Equation for Bound-State Problems”, Physical Review, Vol.84, No.6, 1951.
- [10] J.R. Spence and J.P. Vary, "Electron-proton resonances at low energy from a relativistic two-body wave equation", Physics Letters B 271 (1991) 27-31.
- [11] S. J. Brodsky and R. F. Lebed, Phys. Rev. Lett. 102, 213401, arXiv:0904.2225, 2009.
- [12] S. Flügge, “Practical Quantum Mechanics”, (equation 202.17, page 198), Springer-Verlag, the 2-nd printing, 1994.
- [13] Deck, J. G. Amar, and G. Fralick, “Nuclear size corrections to the energy levels of single-electron and single-muon atoms”, Phys. B: At. Mol. Opt. Phys. 38 (2005) 2173–2186.
- [14] M. Bednar (deceased), Czech Physical Institute, Prague, private communication, July 22, 1997.
- [15] https://en.wikipedia.org/wiki/Virial_theorem
- [16] J. Gaiete, arXiv:1306.0722v1 [hep-th] 4 Jun 2013
- [17] W. Lucha, Mod. Physics Lett., Vol.5, No.30 (1990) 2473-2483.
- [18] J. Va’vra, “A simple argument that small hydrogen may Exist,” Physics Letters B 794 (2019) 130-134., May 27, 2019, updated version in arXiv:1906.08243v4, Dec. 17, 2023.
- [19] E.E. Salpeter and H. Bethe, “Quantum mechanics of one and two electron atoms,” (equation 12.9, page 56) Springer-Verlag, 1957, 2-nd print, 2014.
- [20] P.A.Tipler, “Foundations of Modern Physics”, p. 310, Worth Publishers, Inc., New York 10016, 1969.
- [21] J.L. Paillet and A. Meulenberg, “Advance on Electron Deep Orbits of the Hydrogen Atom”, J. Condensed Matter Nucl. Sci. 24 (2017) 258–277.
- [22] J.L. Paillet and A. Meulenberg, “On Highly Relativistic Deep Electrons,” J. Condensed Matter Nucl. Sci. 29 (2019) 1–21.
- [23] J.L. Paillet and A. Meulenberg, “Deepening Questions about Electron Deep Orbits of the Hydrogen Atom,” J. Condensed Matter Nucl. Sci. 26 (2017) 1–15.
- [24] S. V. Adamenko and V. I. Vysotskii, “Mechanism of synthesis of superheavy nuclei via the process of controlled electron-nuclear collapse,” Foundations of Physics Letters, Vol. 17, No. 3, June 2004.
- [25] Yukawa, H. (1935). "On the interaction of elementary Particles," Proc. Phys. Math. Soc. Jpn. 17: 48.
- [26] G. A. Schott, Phil. Mag. Suppl. 7, 15, 752 (1933).
- [27] G. H. Goedecke, “Classically Radiation-less Motions and Possible Implications for Quantum Theory,” Phys. Rev.,

- Vol 135, No.1B, 1964.
- [28] A. Okninski, "A remark on Zitterbewegung and Schott's Radiationless motion," Technical Report · August 2021, <https://www.researchgate.net/publication/354117700>.
 - [29] A. Barut, A. Bracken, "Zitterbewegung and the internal geometry of the electron." *Physical Review D*, 23 (1981) 2454
 - [30] P. Gibbon, Proceedings of the CAS-CERN Accelerator School: Plasma Wake Acceleration, Geneva, Switzerland, 23 Nov. 2014.
 - [31] Laser tests at NIF LANL, https://en.wikipedia.org/wiki/National_Ignition_Facility
 - [32] J. Va'vra, J. Maly, P.M. Va'vra, "Soft X-ray production in spark discharges in hydrogen, nitrogen, air, argon, and xenon gases," *Nucl. Instr. Meth.*, A 418 (1998) 405, and J. Va'vra, "Soft X-ray production in spark discharges in hydrogen," unpublished work available only in logbooks
 - [33] B. Zheng et al., *Plasma Sources Science and Technology*, July 2019, DOI: 10.1088/1361-6595/ab36a6
 - [34] J. Va'vra, talk at Babar collaboration meeting: "Proposal for a search of small hydrogen atom in the BaBar data", June 13, 2017.
 - [35] T. Enoto et al., "Photonuclear reactions triggered by Lightning discharge," *Nature*, 551, pages 481–484 (2017).
 - [36] J.W. Dwyer and M.A. Uman, "The physics of lightning", *Physics Report* 534 (2014) 147-241.
 - [37] L. Babich, "Thunderous nuclear reactions", *Nature* 551, p.443-444, Nov.22, 2017.
 - [38] G. N. Shah et al., "Neutron generation in lightning bolts", *Nature*, 313, 773-775, 28 February 28, 1985.
 - [39] A.V. Agafonov et al., "Observation of hard radiations in a laboratory atmospheric high-voltage discharge", arXiv:1604.07784v1 [physics.plasma-ph], April 26, 2016.
 - [40] N. Prantzos et al., "The 511 keV emission from positron annihilation in the Galaxy", *Rev. Mod. Phys* 83, 1001 (2011) <https://doi.org/10.1103/RevModPhys.83.1001>, arXiv:1009.4620.
 - [41] P. Martin et al., "Galactic annihilation emission from nucleosynthesis positrons," ArXiv:1205.1194, Nov.9, 2018.
 - [42] C. Bambi, A. D. Dolgov A. A. Petrov, "Primordial black holes and the observed Galactic 511 keV line," *Physics Letters B* 670 (2008) 174–178.
 - [43] Y. Ema, F. Sala, and R. Sato, "Dark matter models for the 511 keV galactic line predict keV electron recoils on Earth," *Eur. Phys. J. C* (2021) 81:129, <https://doi.org/10.1140/epjc/s10052-021-08899-y>.
 - [44] G. Weidenspointner et al., *Astronomy and Astrophysics* 411, L113L11 (2003).
 - [45] Bass2000 Solar Survey Archive, http://bass2000.obspm.fr/solar_spect.php
 - [46] W. Curdt et al., "The summer spectral atlas of solar disk features", *Astronomy & Astrophysics*, June 4, 2004.
 - [47] Hitoshi Muayama, 221A lecture notes, University of California, Berkeley, USA, <https://guide.berkeley.edu/courses/physics/>
 - [48] W. Zawadzki, "Spin Magnetic Moment of a free Electron", *Phys.Rev.D*, Vol.3, No.8, April 15, 1971.
 - [49] M.T. Ressel, M.S. Turner, M.A. Bershad: *Bulletin of the American Astronomical Society*: Vol. 22, September 1, 1990.
 - [50] M.T. Ressel and M.S. Turner, *Comm. on Astrophysics*, 14 (1990) 323.
 - [51] R.J. Bouwens et al., "A candidate redshift $z \sim 10$ galaxy and rapid changes in that population at an age of 500 Myr," *Nature*, page 504, Vol. 469, Jan.27, 2011, and ArXiv:0912.4263 [Astro-ph.CO], Jan.30, 2011.
 - [52] R. Genzel et al., *Nature*, 543, 397–401 (16 March 2017).
 - [53] R. Wagoner, private communication 2024, and 1973, *Ap.J.*, **179**,343.
 - [54] Adhikari et al., "Astrophysical Tests of Dark Matter Self-Interactions," arXiv:2207.10638v1 [astro-ph.CO], July 21, 2022.
 - [55] D. Harvey et al., arXiv:1503.07675 [astro-ph.CO], March 26, 2015.
 - [56] JANIS software, <https://www.oecd-neo.org/janis>, 2020.
 - [57] https://en.wikipedia.org/wiki/Neutron_cross_section, which is also using JANIS software.
 - [58] F. Metzler, C. Hunt, P. L. Hagelstein and N. Galvanetto, *New J. Phys.* 26 (2024) 101202.